

Towards the Emulation of the Cardiac Conduction System for Pacemaker Testing

Eugene Yip, Sidharta Andalam, Partha S. Roop, Avinash Malik, Mark Trew, Weiwei Ai, and Nitish Patel

Abstract—The heart is a vital organ that relies on the orchestrated propagation of electrical stimuli to coordinate each heart beat. Abnormalities in the heart’s electrical behaviour can be managed with a cardiac pacemaker. Recently, the closed-loop testing of pacemakers with an emulation (real-time simulation) of the heart has been proposed. An emulated heart would provide realistic reactions to the pacemaker as if it were a real heart. This enables developers to interrogate their pacemaker design without having to engage in costly or lengthy clinical trials. Many high-fidelity heart models have been developed, but are too computationally intensive to be simulated in real-time. Heart models, designed specifically for the closed-loop testing of pacemakers, are too abstract to be useful in the testing of physical pacemakers.

In the context of pacemaker testing, this paper presents a more computationally efficient heart model that generates realistic continuous-time electrical signals. The heart model is composed of cardiac cells that are connected by paths. Significant improvements were made to an existing cardiac cell model to stabilise its activation behaviour and to an existing path model to capture the behaviour of continuous electrical propagation. We provide simulation results that show our ability to faithfully model complex re-entrant circuits (that cause arrhythmia) that existing heart models can not.

Index Terms—cardiac, electrophysiology, emulation, hybrid, automata, modelling.

I. INTRODUCTION

The human heart is a vital organ and is responsible for pumping blood around the body to other vital organs. Patients can develop abnormal cardiac behaviour, such as bradycardia (slow heart rate). Cardiac pacemakers can treat bradycardia by monitoring the patient’s heart and delivering electrical stimuli to the heart when needed. Pacemakers are life-critical medical devices that must be certified against stringent safety standards, such as IEC 60601-1 [1]. Certification is a costly and time consuming process, yet 1,210 computer-related recalls for medical devices were reported to the US Food and Drug Administration between 2006 and 2011 [2].

Pacemakers must be validated by clinical trials as part of the certification process. This requires the pacemaker to be tested in closed-loop with a patient’s heart. Since clinical trials are the only times when a pacemaker is tested on a real heart, they provide a glimpse of how well the pacemaker performs in the real world. Clinical trials are usually performed late in the product development phase, because they are costly and time

consuming to manage. Thus, issues found during a clinical trial may be costly and time consuming to fix and a new clinical trial may be required to re-evaluate the pacemaker. Some limitations of clinical trials include: potentially small sample of patients that are not representative of the general population, difficulty in recruiting patients with specific heart conditions, difficulty in interrogating a patient’s heart to better understand design issues, and inherent risk to the patients.

Recently, the emulation of the heart has been proposed to facilitate the closed-loop testing of pacemakers [3]. Emulation is the real-time simulation of a heart model that can react to a pacemaker’s electrical shocks and also output the heart’s electrical activities for the pacemaker to sense. High-fidelity heart models provide realistic behaviour but are computationally intensive [4], [5], thus, precluding them from emulation. The following benefits can be gained if high-fidelity heart models can be emulated: cheaper and quicker testing than with clinical trials, earlier testing of pacemakers in closed-loop in the development phase and outside of clinics, greater testing coverage by emulating a range of heart conditions, better understanding of design issues by interrogating the emulated heart (e.g., replaying problematic test cases), and having minimal risk to the patients. We envision the use of emulated hearts alongside clinical trials to help accelerate the certification process.

In the context of testing cardiac pacemakers, a heart model should possess the following properties:

- **Abstraction:** The model focusses on the important aspects by ignoring irrelevant details. For example, the cardiac conduction system is the most important aspect because it is responsible for coordinating the heart’s electrical activities. Irrelevant details may include hemodynamics (e.g., blood flow), mechanics (e.g., muscle movement), and chemistry (e.g., cellular reactions).
- **Accuracy:** The model faithfully represents the cardiac conduction system and demonstrates realistic behaviours. A high-fidelity model provides an accurate reflection of reality but requires high computational power. A lower fidelity model requires less computational power but at the risk of providing an inaccurate reflection of reality.
- **Prediction:** The model can answer questions about a real heart, such as “How does the heart respond when setting X of the pacemaker is used?”
- **Inexpensiveness:** The model should be cheaper and faster to construct and use the emulated heart than to conduct a clinical trial.

The heart models of Chen et al. [6], Jiang et al. [7], and

E. Yip was and S. Andalam, P. S. Roop, A. Malik, W. Ai, and N. Patel are with the Department of Electrical and Computer Engineering, the University of Auckland, New Zealand. M. Trew is with the Auckland Bioengineering Institute, the University of Auckland, New Zealand.

E-mails: {eyip002, wai484}@aucklanduni.ac.nz and {sid.andalam, p.roop, avinash.malik, nd.patel, m.trew}@auckland.ac.nz

Méry and Singh [8] consider just the emergent features of the cardiac conduction system, which is composed of millions of cells. They model the conduction system as a static, two-dimensional, sparse network of cardiac cells. Jiang et al. [3] also developed a hardware prototype that emulates the cardiac conduction system as discrete events. When the logic of a pacemaker's software is tested in closed-loop with a heart model, it may be sufficient to use a heart model that produces and responds to discrete events [7], [8]. However, when a physical implementation of the pacemaker is tested in closed-loop with a heart model, it is necessary to use a heart model that produces and responds to continuous-time signals. This is because the physical pacemaker expects a real heart as its environment. The heart model of Chen et al. [6] simulates the conduction system as continuous-time signals. However, the signals are too abstract and bear little resemblance with reality. Thus, the model lacks the accuracy and, therefore, the predictive power.

A. Contributions

This paper reviews the state-of-the-art heart models [3], [6]–[9] that have been designed specifically for the closed-loop testing of cardiac pacemakers. Without introducing significant computational complexity, we propose significant improvements to the modelling of the cardiac conduction system to create a heart model that produces realistic continuous-time electrical signals that a pacemaker would sense. Our model faithfully models forward and backward conduction, which is essential in the modelling of complex re-entrant circuits [10]–[12] that cause arrhythmia (abnormal heart rate). Our primary contributions are:

- We develop a continuous-time model of the conduction system as a two-dimensional network of cardiac cells. Each cell produces an accurate continuous-time signal that represents its electrical activities. These signals are propagated continuously along the paths between the cells. Complex conduction behaviours, such as arrhythmias caused by re-entrant circuits, can be reproduced faithfully by our model. Our heart model is easily customised by modifying various parameters of the conduction system.
- Each cardiac cell in our heart model is based on the hybrid automaton developed by Ye et al. [13]. We have greatly improved the design of the hybrid automaton to overcome the following limitations: the cell becomes unstable when it is stimulated in quick succession, and the cell is too sensitive to electrical stimulation from its neighbours. Our improvements are elaborated in Section IV.
- Each path in our heart model is modelled with timed automata. The path model is inspired by that of Jiang et al. [7] that was designed to propagate discrete events rather than continuous-time signals. Our path model is elaborated in Section V.
- We demonstrate in Section VII that a MathWorks® Simulink® and Stateflow® implementation of our heart model can simulate a wide range of heart conditions with realistic results.

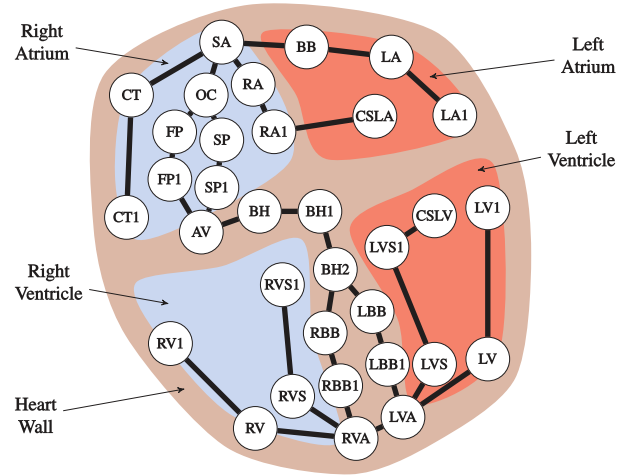


Fig. 1. Schematic of the heart and conduction system.

B. Paper Layout

Section II provides a background to the cardiac conduction system and the important features of electrical activities that are sensed by a pacemaker. Section III reviews the state-of-the-art heart models for closed-loop testing of pacemakers. Section IV reviews the computationally efficient hybrid automata model of cardiac cells developed by Ye et al. [13]. We identify the limitations encountered with Ye et al.'s model during simulation and how we corrected them. Section V describes our path model that handles the propagation of continuous-time signals. In Section VI, we create our proposed heart model by composing instances of our cardiac cell and path models into a network that replicates the conduction pathway. Section VII evaluates the capabilities of our proposed heart model with the recent heart model of Chen et al. [6]. Section VIII concludes this paper and discusses future work for improving the proposed heart model.

II. BACKGROUND

The heart pumps blood around the body in a rhythmic manner. Figure 1 is a schematic of the heart and shows its four chambers: the right and left atriums and ventricles. The right atrium and ventricle are responsible for pumping deoxygenated blood through the lungs, while the left atrium and ventricle are responsible for pumping oxygenated blood through the body. The contractions of the chambers are coordinated by electrical stimuli that propagate throughout the heart's conduction system. The conduction pathways are shown in Figure 1 as solid black lines with dots at important locations. The names of these locations are labelled with an acronym and their full forms are given in Table I.

A. Cardiac Cycle

This section describes the major actions of the heart during one cardiac cycle (one heart beat) with the help of Figure 2. In the first phase of the cardiac cycle, Figure 2a, the sinoatrial (SA) node generates an electrical stimulus that spreads quickly throughout the right and left atriums. This causes

TABLE I
FULL NAMES OF NODES ALONG THE CONDUCTION PATHWAYS.

AV	Atrioventricular	LVS	Left ventricular septum
BB	Bachmann's bundle	OC	Os cordis
BH	Bundle of His	RA	Right atrium
CS	Coronary sinus	RBB	Right bundle branch
CT	Crista terminalis	RV	Right ventricle
FP	Fast path	RVA	Right ventricular apex
LA	Left atrium	RVS	Right ventricular septum
LBB	Left bundle branch	SA	Sinoatrial
LV	Left ventricle	SP	Slow path
LVA	Left ventricular apex		

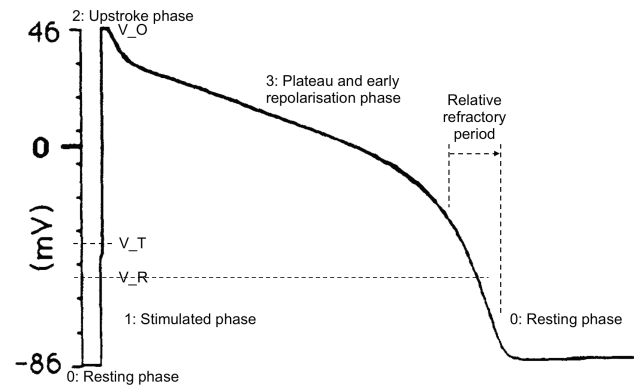


Fig. 3. Phases of the action potential. Adapted from [14].

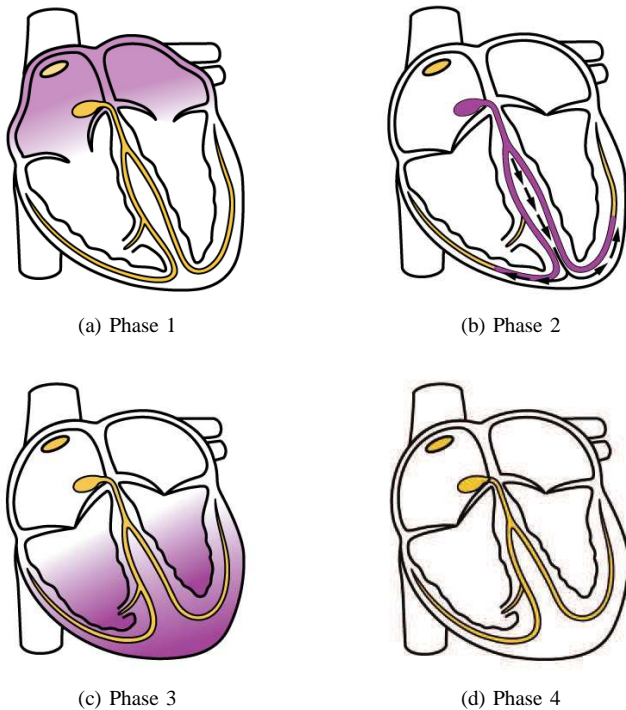


Fig. 2. Phases of the cardiac cycle. Adapted from <http://philschatz.com/anatomy-book/contents/m46664.html#sinoatrial-sa-node>.

the atriums to contract, pumping blood from the atriums into the ventricles. In the second phase, Figure 2b, the electrical stimulus reaches the atrioventricular (AV) node and is delayed momentarily before it continues down into the ventricles. This delay is very important because it gives the atriums enough time to contract and fully fill the (relaxed) ventricles. In the third phase, Figure 2c, the electrical stimulus reaches the right and left ventricular apices and travels out to the fast conducting Purkinje fibers. This causes the right and left ventricles to contract and pump out blood. In the fourth phase, Figure 2d, the ventricles relax after pumping out all their blood.

In a normal heart, each cardiac cycle begins from the SA node, which generates periodic electrical stimuli that spread through the conduction system. The following sections describe the genesis of the heart's electrical activity and how it appears to a pacemaker. Finally, we describe some common

arrhythmias that a heart model should aim to capture.

B. Action Potentials of Cardiac Cells

Most of the heart's electrical activities, that a pacemaker senses, are generated by the myocytes (muscle cells) [15]. A cell's electrical activities result from the movement of ions across its membrane, creating potential differences. The cell's electrical response to an electrical stimulus is described by its *action potential* [16]. Figure 3 shows the four phases of a typical action potential, which plots the cell's membrane potential over time. In the **resting phase**, the cell is inactive and has a resting potential of approximately $-85mV$. The cell enters the **stimulated phase** when excited electrically by its neighbours or by an artificial pacemaker. The cell returns to the resting phase if its membrane potential fails to cross the threshold voltage V_T of approximately $-40mV$ when the excitation stops. Otherwise, the cell enters the **upstroke phase** and *depolarises* by allowing ions to move rapidly across its membrane, causing its membrane potential to reach an overshoot voltage V_O of approximately $+45mV$. Then the cell enters the **plateau and early repolarisation phase**. The cell contracts and starts to *repolarise*, i.e., its membrane potential starts to return to its resting potential. When the membrane potential is less than the voltage V_R of approximately $-55mV$, the cell has relaxed and returned to the resting phase.

All cardiac cells can only respond to subsequent excitations in the later portion of its action potential, called the *relative refractory period*. However, the membrane potential must cross a higher threshold voltage. Figure 4 shows a normal action potential at $0ms$ and some possible secondary excitations between 160 and $300ms$. For a secondary excitation at $180ms$, the resulting action potential has a lower overshoot voltage V_O and a shorter action potential duration. The secondary excitation at $300ms$ results in a more normal action potential because the cell has rested for a longer period.

Prominent biophysical cardiac cell models, which explain the genesis of action potentials in terms of ionic flow, include Luo-Rudy [16] and Hodgkin-Huxley [18]. Although biophysical models have high-fidelity, they are computationally intensive. Ye et al. [13], [19] create computationally efficient cardiac cell models by considering just the emergent features of the biophysical models, i.e., the action potential

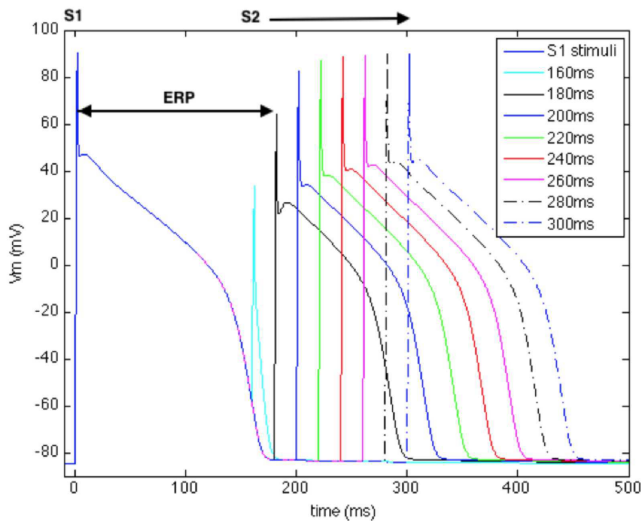


Fig. 4. Dynamic behaviour of secondary excitations. Adapted from [17].

and its dynamic response to secondary excitation. It should be noted that the action potential duration of a human ventricular myocyte is approximately twice that of an atrial myocyte.

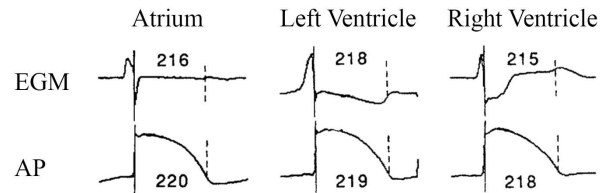
C. Action Potentials and the Electrogram

A key function of any pacemaker is to sense the heart's electrical activity, by using one or more electrodes attached to the inside of the heart wall. The electrical activity of the cardiac cells in the electrode's immediate vicinity are sensed most strongly. A recording of the sensed activities is called an electrogram (EGM) [20]. Figure 5a shows three action potentials and their corresponding EGMs. To help understand the EGM, Figure 5b shows that the EGM deflects up and down whenever an electrical wavefront passes under the electrodes [15]. The faster that the wavefront passes, the steeper the deflection. In Figure 5a, two distinct deflections can be seen in each EGM and they correspond with the upstroke and resting phases of their respective action potential.

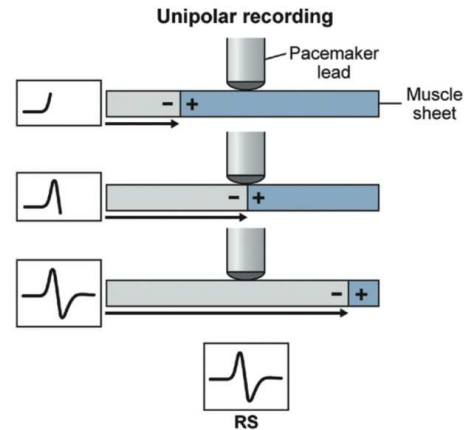
A heart model that produces distorted action potentials will also produce distorted EGMs. Such distorted EGMs cannot be used to reliably test a pacemaker's ability to discern the timing of important cardiac activities. Moreover, the predictive power of a heart model is compromised when the action potentials are distorted. For example, a heart model with accurate action potentials might predict that a cell goes into its upstroke phase because its neighbours' voltages are high enough. However, a heart model with distorted action potentials might instead predict that the cell returns to its resting phase because its neighbours' voltages are too low. Thus, arrhythmia would be predicted incorrectly.

D. Common Arrhythmias

Arrhythmias can be caused by abnormalities in the generation and propagation of action potentials through the conduction system. The abnormalities may be due to congenital defects, side-effects of medication, or cell death. The following



(a) Three action potentials (APs) from different regions of the heart and their corresponding electrograms (EGMs). Adapted from [21].



(b) EGM deflections due to a travelling electrical wavefront. Adapted from [15].

Fig. 5. Electrograms (EGMs).

are some common arrhythmias [11], [12], [20] that a heart model for pacemaker testing should aim to capture:

- **Heart block:** This occurs when electrical stimuli has difficulty propagating through the AV node. The propagation of the stimuli may be delayed for longer than usual or may be prevented from propagating altogether.
- **AV node re-entrant tachycardia:** This occurs when a re-entry circuit forms around the AV node, causing tachycardia.
- **Bundle branch block:** This occurs when electrical stimuli travels slower or not at all down one of the bundle branches.
- **Wolff-Parkinson-White syndrome:** This occurs when there is an extra conduction pathway between the atriums and ventricles. The extra pathway allows electrical stimuli to bypass the AV node and create a feedback loop between the atriums and ventricles.
- **Long Q-T syndrome:** This occurs when the repolarisation of the ventricles is delayed, i.e., their action potential durations are longer than usual.
- **VA conduction:** This occurs when electrical stimuli from the ventricles conduct backwards through the conduction pathways and into the atriums.

Pacemakers can also cause arrhythmias when they are unable to correctly sense the timing of the heart's electrical activities. For example, pacemaker-mediated tachycardia is caused by the pacemaker inadvertently conducting electrical stimuli from the ventricles back to the atriums. Pacemakers that deliver electrical stimuli that are not synchronised with

TABLE II
 QUALITATIVE COMPARISON OF HEART MODELS THAT ARE DESIGNED FOR TESTING CARDIAC MEDICAL DEVICES. AP = ACTION POTENTIAL. HA = HYBRID AUTOMATA. TA = TIMED AUTOMATA.

	Reality	Less Abstract ←	Heart Models				→ More Abstract
	Real Heart [22]	Hi-Fi [23], [24]	UoA	Oxford [6]	UPenn [3], [7]	LORIA [8]	MES [9]
Cell Model	Continuous APs from biophysical processes [25]	Continuous APs from biophysical models [25]	Continuous APs from improved Stony Brook HA [13]	Continuous APs from simplified Stony Brook HA [19]	Discrete APs from TA	Discrete APs from logico-mathematics	Continuous AV signal generators mimic whole heart electrical activity
Path Model	Continuous propagations from biophysical processes [10]	Continuous propagations from reaction-diffusion equations [25]	Continuous propagations from TA and contribution function	Continuous propagations from contribution function	Discrete propagations from TA	Discrete propagations from cellular automata	
Spatial Model	3D tissue (layers of bundles of fibers) that deforms	3D finite-volume that deforms	2D, static, and sparse network of cells along the conduction pathway				Black boxes of major heart components

the heart's cardiac rhythm can cause the heart to fibrillate [26], i.e., twitch uncontrollably.

III. RELATED WORK

The electrophysiology of the heart has been well researched [10], [27], resulting in the proposal of many theories. These theories are validated by creating high-fidelity whole heart models [23], [24] and ascertaining if they can reproduce experimental observations, i.e., the models are accurate, realistic, and predictive. These high-fidelity models are useful in predicting the prognosis of patient-specific heart conditions [28] and in assisting with interventional cardiology [29].

On the other hand, abstract heart models have been developed with the goal of enabling the closed-loop testing of cardiac pacemakers. Table II provides a qualitative comparison of existing heart models. The abstract heart models from Oxford [6], UPenn [3], [7], LORIA [8], and MES [9] are designed for testing the pacemaker logic. To enable the formal verification of the pacemaker logic, Oxford, UPenn, and LORIA use hybrid automata (HA) or timed automata (TA) to develop formal models of the cardiac conduction system. UPenn and LORIA model the transitions between the resting, upstroke, and early refractory phases of the action potential as discrete events on a continuous timeline. These discrete events are propagated between cells and the propagation is either successful or unsuccessful. These abstractions result in heart models that may produce more behaviours than is possible by a real heart, i.e., an over-approximation. Thus, all problems detected during closed-loop testing must be validated against a more concrete heart model [7].

The heart model from Oxford [6] is more concrete than those from UPenn and LORIA because Oxford models the action potentials as continuous signals. Oxford uses a simplified model of the cardiac cell that Ye et al. [19] developed with hybrid automata. Oxford incorporates a $g(\vec{v})$ function into the cell model to capture the continuous electrical activity that a cell receives from its neighbours. However, the $g(\vec{v})$ function does not consider the directional behaviour of electrical propagation due to the refractory period of cardiac cells. Noting these limitations, Sections IV and V describe our

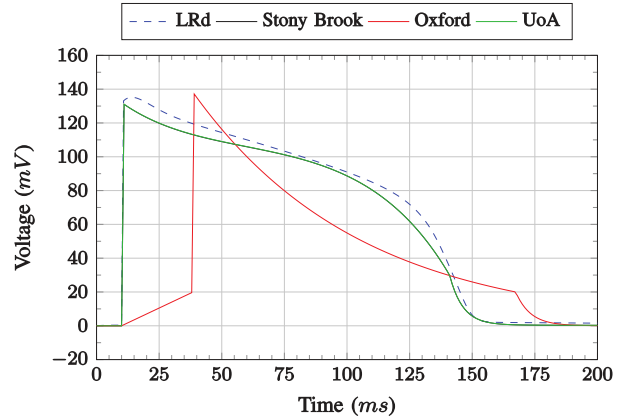


Fig. 6. Comparison of the action potentials (APs) produced by Luo-Rudy [16], Stony Brook [13], Oxford [6], and our improved version (UoA). Note that the AP of UoA overlaps that of Stony Brook's because they are identical.

improvements to the cell and path models. Our heart model can faithfully simulate complex re-entrant circuits without a significant increase in computational complexity.

IV. CARDIAC CELL MODEL

The Oxford heart model [6] uses a simplified version of the isolated cardiac cell model developed by Stony Brook [19]. The Stony Brook model is itself a simplification of the Luo-Rudy model [16] because it only models the action potential and its dynamic response to secondary excitation. The Stony Brook model uses three piecewise-continuous variables, called v_x , v_y , and v_z , to capture different features of the action potential. The sum of these three variables produces the action potential. The Oxford heart model discards the v_y and v_z variables and retains just the v_x variable. Unfortunately, Figure 6 shows that the resulting action potential is no longer realistic and this diminishes the predictive power of Oxford's heart model (Section II-C). Thus, for our heart model, we retain all three variables and we use an updated Stony Brook cardiac cell model [13]. This section describes the Stony Brook model in more detail and our improvements that overcome some of the model's limitations.

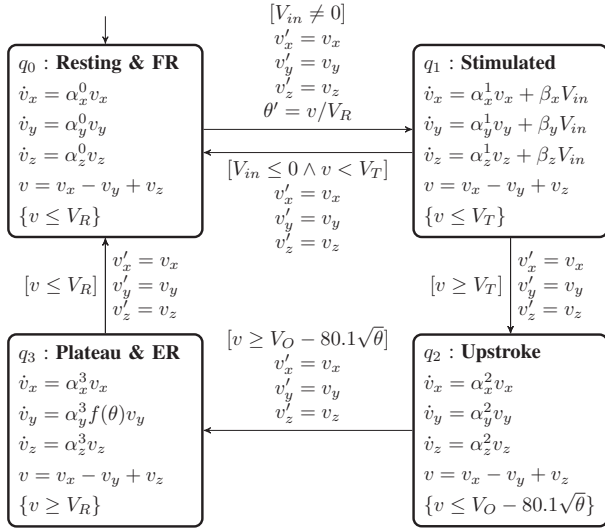


Fig. 7. Stony Brook cardiac cell model [13].

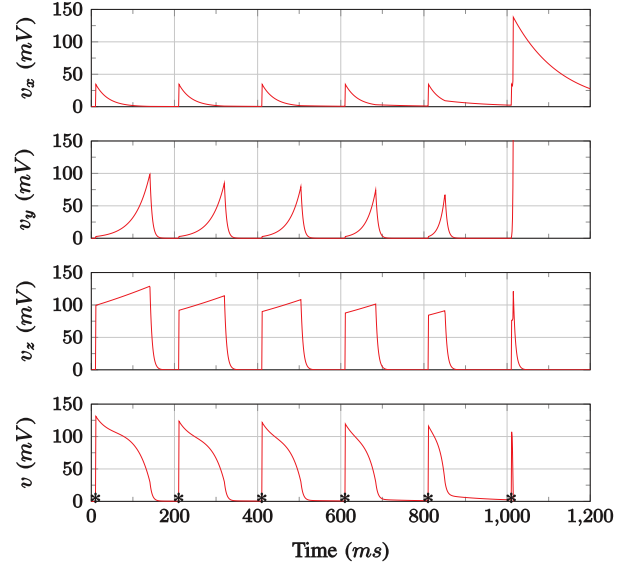
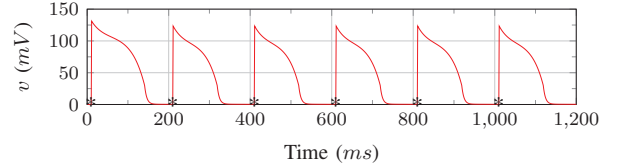
TABLE III
COEFFICIENTS AND CONSTANTS IN THE STONY BROOK CARDIAC CELL MODEL [13].

$\alpha_x^0 = -0.0087$	$\alpha_x^1 = -0.0236$	$\alpha_x^2 = -0.0069$	$\alpha_x^3 = -0.0332$
$\alpha_y^0 = -0.1909$	$\alpha_y^1 = -0.0455$	$\alpha_y^2 = 0.0759$	$\alpha_y^3 = 0.0280$
$\alpha_z^0 = -0.1904$	$\alpha_z^1 = -0.0129$	$\alpha_z^2 = 6.8265$	$\alpha_z^3 = 0.0020$
$V_R = 30$	$\beta_x = 0.7772$		
$V_T = 44.5$	$\beta_y = 0.0589$		
$V_O = 131.1$	$\beta_z = 0.2766$		

A. Stony Brook Cardiac Cell Model

The Stony Brook model [13] models the time course of the action potential with the *hybrid automaton* (HA) shown in Figure 7. The four phases of the action potential, described in Section II-B, are represented as four locations in the HA. In each location, the membrane potential is defined by the variable v as the sum of the variables v_x , v_y , and v_z . The rates at which the variables v_x , v_y , and v_z change are defined by their derivatives \dot{v}_x , \dot{v}_y , and \dot{v}_z , respectively. The values of the coefficients and constants are given in Table III. Note that the Stony Brook model offsets all the voltages such that the resting potential is at $0mV$.

By default, the HA always starts in location q_0 , which is the resting phase of the action potential. It stays in q_0 as long as the invariant $v \leq V_R$ is true. The HA transitions from location q_0 to q_1 when the voltage V_{in} around the cell is greater than $0mV$. During this transition, the last values of v_x , v_y , and v_z when leaving q_0 are used to set their initial values when entering q_1 . Recall from Figure 4 that the amplitude and duration of the action potential depends on how long the cell had been in the resting phase when it is stimulated. This is approximated by assuming that the closer the cell's membrane potential is to $0mV$, the longer the cell has been in location q_0 . Thus, the time that the cell had been in the resting phase is approximated by normalising the membrane potential v against the voltage V_R , i.e., $\theta = v/V_R$. In location q_1 , the rate at

Fig. 8. Action potentials shorten unnaturally for the Stony Brook model. Stimulated at $200ms$ intervalsFig. 9. Action potentials for the UoA model when stimulated at $200ms$ intervals.

which the cell's membrane potential increases depends on the strength of V_{in} . The HA transitions back to location q_0 if the voltage V_{in} around the cell fails to stimulate the cell above the threshold voltage V_T . However, if the cell's membrane voltage v is stimulated above V_T , then the HA transitions to location q_2 . The amplitude of the cell's membrane potential is calculated as $V_O - 80.1\sqrt{\theta}$, i.e., it depends on how long the cell had been in the resting phase. The HA transitions to location q_3 and the cell's membrane potential starts to drop. The rate of repolarisation is determined by the function $f(\theta)$ and depends on how long the cell had been in the resting phase:

$$f(\theta) = 0.29e^{62.89\theta} + 0.70e^{-10.99\theta} \quad (1)$$

A higher value for $f(\theta)$ means a faster rate of repolarisation. Once the cell's membrane voltage v drops below the resting voltage V_R , the HA transitions back to q_0 .

B. Improvement: Stabilising the Action Potential

The bottom plot in Figure 8 shows the action potentials produced by the Stony Brook model when stimulated at $200ms$ intervals. We can see that the duration of the action potentials shorten towards zero over time. This is unnatural because the action potentials should settle to a constant duration when stimulated at a constant interval [30]. The top three plots in Figure 8 show the values of v_x , v_y , and v_z , respectively, over time. Note that v_x describes the initial voltage drop of the

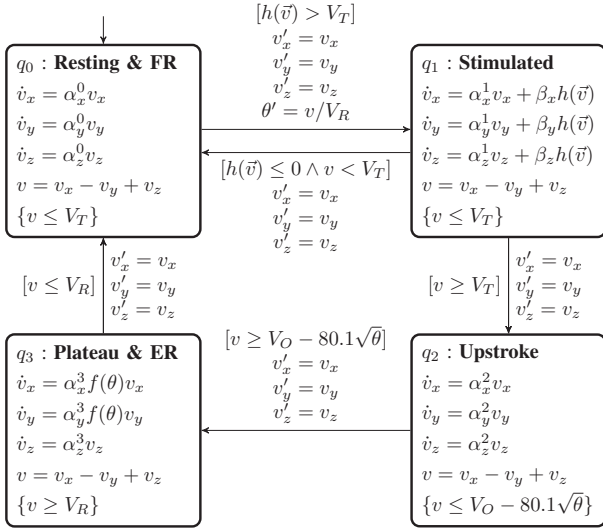


Fig. 10. Improved cardiac cell model (UoA).

plateau phase. We can see that the v_x variable takes too long to decrease in location q_0 . Thus, each time the cell is stimulated, it enters location q_1 with a slightly higher value for v_x . This causes the values of θ and $f(\theta)$ to increase over time. An increasing value of $f(\theta)$ causes a faster rate of repolarisation and, hence, shorter action potential durations.

To prevent the unnatural shortening of the action potential, the value of v_x needs to be closer to zero when the cell transitions from location q_3 to q_0 . Thus, we increase the rate at which v_x decreases towards zero by including the function $f(\theta)$ in location q_3 for \dot{v}_x . The improved HA is shown in Figure 10. Figure 9 shows that the action potentials produced by the improved HA have constant durations when stimulated at 200ms intervals.

C. Improvement: Bounding the Rate of Repolarisation

In the Stony Brook model, the action potential duration approaches zero if the cell was stimulated shortly after entering location q_0 . This behaviour is unnatural because the minimum action potential duration that a cardiac cell can achieve is approximately 40ms. This problem is due to the function $f(\theta)$. When the HA returns to location q_0 from q_3 , the value of v is V_R . An immediate stimulation to location q_1 would set $\theta = V_R/V_R = 1$. Consequently, $f(1) = 5.96 \times 10^{26}$, which causes an extremely fast rate of repolarisation.

To prevent such a fast rate of repolarisation from occurring, we limit the maximum value that function $f(\theta)$ can return. Figure 11 shows that action potential durations of 35 ms are produced when $f(\theta = 0.04) = 4.0395$. Thus, we impose a maximum value of 4.0395 for the function $f(\theta)$:

$$f(\theta) = \begin{cases} 0.29e^{62.89\theta} + 0.70e^{-10.99\theta} & \text{if } \theta < 0.04 \\ 4.0395 & \text{if } \theta \geq 0.04 \end{cases}$$

D. Discussion

We improved the original Stony Brook cardiac cell model [13] to stabilise the action potentials and to impose

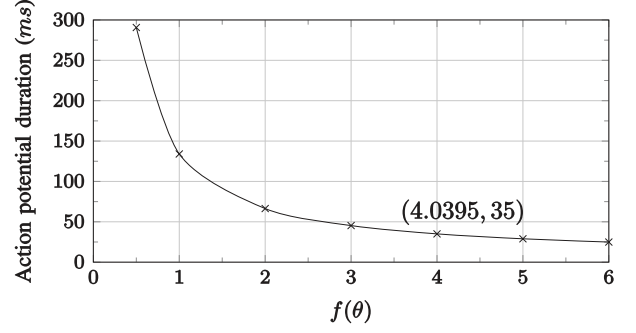


Fig. 11. Relationship between the action potential duration (APD) and the value of $f(\theta)$.

a reasonable minimum action potential duration. Figure 9 shows that the shape of the action potentials generated by the improved model remains realistic. However, it is important to demonstrate that the action potential durations vary realistically in response to the timing of secondary excitations (see Figure 4 for illustration). This dynamic behaviour can be evaluated with a restitution curve [30]. To plot the restitution curve, the cardiac cell is electrically stimulated at a constant time period, called the base cycle length (BCL). The BCL consists of two time intervals: the action potential duration followed by the *diastolic interval*. The diastolic interval begins when the action potential falls to 10% of its peak amplitude. For a range of BCLs, the action potential duration from the tenth BCL is plotted against the diastolic interval from the ninth BCL.

Figure 12 shows the restitution curves for the Stony Brook [13], Oxford [6], and our improved (UoA) models. These models were implemented in MathWorks[®] Simulink[®]/Stateflow[®]. The Oxford implementation was provided by the original authors [6]. The restitution curve of the Stony Brook model has been demonstrated [13] to behave realistically compared to the Luo-Rudy model. However, because the Stony Brook model is unstable, we could only reproduce its restitution curve by taking the action potential duration and diastolic interval of the first BCL. The restitution curve for our improved model shows dynamic behaviour that is very similar to Stony Brook. The difference is due to the changes described in Section IV-B. The parameters in the cell model can be tuned to produce a variety of restitution curves and is particularly useful when modelling diseased cardiac cells. The Oxford model, on the other hand, shows unrealistic behaviour. The action potential duration is either 9ms or 98ms, depending on whether the diastolic interval is greater or less than 51ms.

V. CARDIAC PATH MODEL

The Oxford heart model [6] models the conduction system as a sparse network of cells (Figure 1). The cells are connected electrically by a voltage contribution function $g_k(\vec{v})$, which calculates the voltage induced at cell k by its neighbours:

$$g_k(\vec{v}) = \sum_{i=1}^n v_i(t - \delta_{ki})a_{ki} - v_k d_k \quad (2)$$

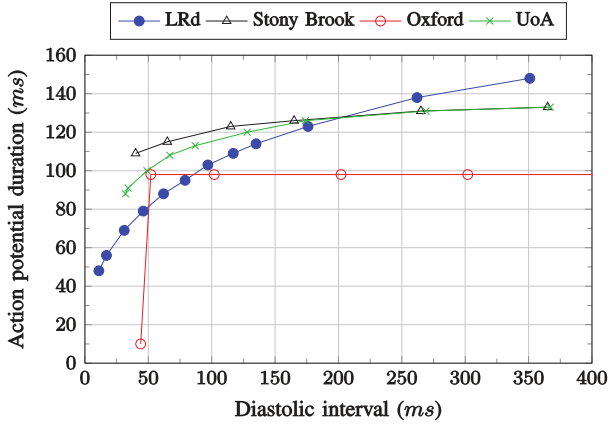


Fig. 12. Electrical restitution curves comparing the dynamic behaviour of Luo-Rudy [16], Stony Brook [13], Oxford [6], and our improved version (UoA).

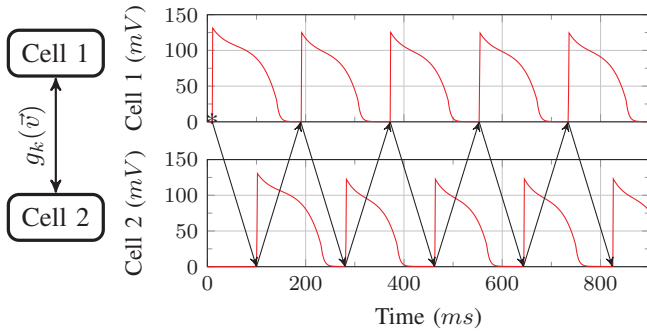


Fig. 13. Two cardiac cells connected electrically by the Oxford voltage contribution function $g_k(\vec{v})$.

For a given cell k with n connected neighbours, $\vec{v} = (v_1 \cdots v_n)$ is a vector of all the neighbours' membrane potentials, such that v_i is the membrane potential of neighbour i . The membrane potential of cell k is v_k . The time for cell i 's action potential to propagate to cell k , called the *conduction time*, is represented by δ_{ki} . Thus, $v_i(t - \delta_{ki})a_{ki}$ represents the membrane potential of cell i that reaches cell k after a delay of δ_{ki} and with a gain of a_{ki} . The strength of cell k 's membrane potential relative to its neighbours is taken into account by $v_k d_k$, where d_k is a distance coefficient.

Figure 13 plots the action potentials of two cardiac cells connected by Oxford's function $g_k(\vec{v})$. Only cell 1 receives an external stimulus at $10ms$ and the time delay between the cells is $90ms$. The expected behaviour is for cell 1 to produce an action potential that stimulates cell 2 to produce an action potential. Cell 2's action potential would not propagate back to cell 1 because of the refractory feature of cardiac cells [11]. However, Figure 13 shows that both cells produce a sequence of action potentials. This is because the term $v_i(t - \delta_{ki})$ in equation (2) requires cell 2's action potential to be propagated back to cell 1 after a time delay. This incorrect positive feedback behaviour is shown in Figure 13 as arrows between the action potentials.

To properly model the propagation of action potentials along a path, its behaviour in real cardiac tissue needs to be reviewed.

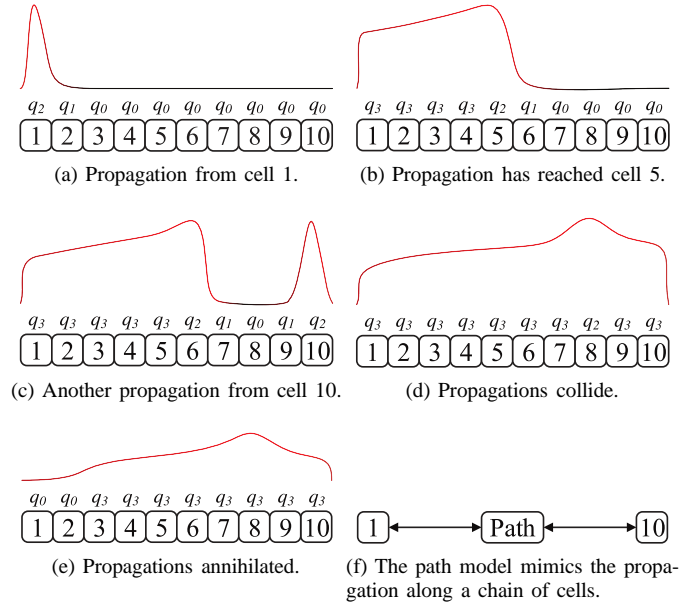


Fig. 14. Propagation and collision of electrical stimuli along cardiac tissue.

Figure 14a shows a chain of cardiac cells where only cell 1 has entered its upstroke phase. The cells' membrane potentials are plotted above the cells along with their corresponding HA location. In Figure 14a, cell 1's membrane potential starts to stimulate cell 2 to enter the upstroke phase. Cell 2 will then stimulate its neighbour and so on. In Figure 14b, cell 5 enters the upstroke phase, while cells 1 to 4 have entered the plateau and early repolarisation phase. Cells 1 to 4 are unresponsive to any electrical stimuli applied to them. This refractory feature forces an action potential to propagate in one direction along a path. When two action potentials propagate towards each other (Figures 14c), they will collide (Figure 14d) and annihilate each other (Figure 14e), i.e., the action potentials will not pass through each other.

A computationally efficient heart model can be created by replacing chains of cardiac cells with paths that mimic the propagation of action potentials (Figure 14f). The path model of UPenn [7] does consider the refractory feature of cardiac cells and can model the collision of electrical stimuli. However, only the propagation of discrete action potential events, rather than continuous-time signals, are modelled. Moreover, a cell can only be stimulated by the electrical activity of one neighbour at a time. We propose a new path model that handles the collision of continuous-time action potentials and calculates the overall voltage induced by a cell's neighbours with a reaction-diffusion [10] function.

A. Improved Path Model

Our *timed automaton* (TA) for determining whether an action potential can propagate along a path is shown in Figure 15a. To keep the path model simple, we assume that the path is only long enough for one complete action potential to propagate through. That is, we assume that the duration of the propagating action potential is longer than its conduction

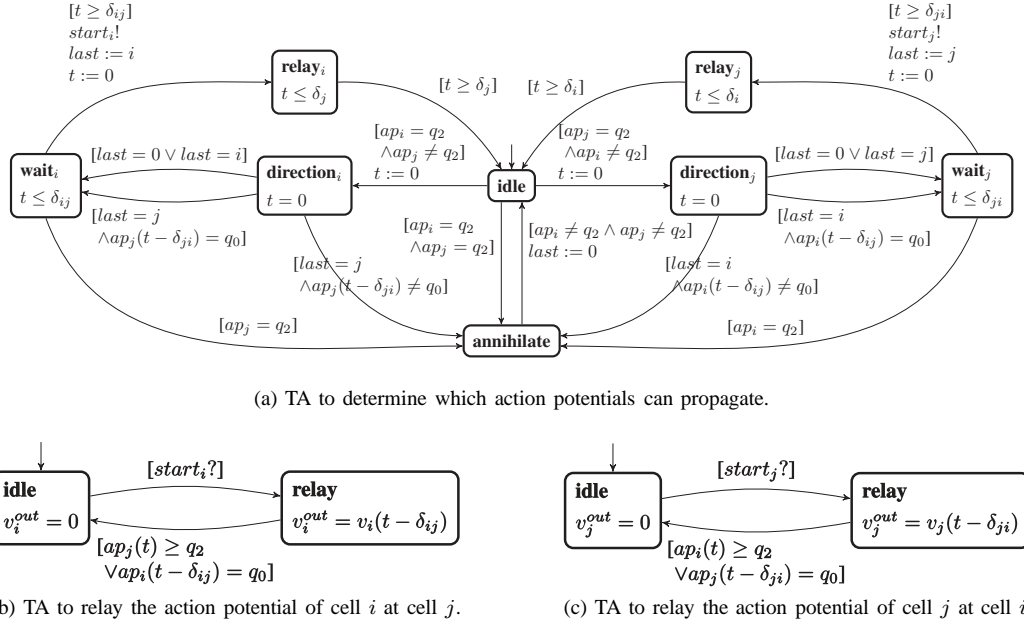


Fig. 15. Improved path model (UoA) consisting of a TA to detect collisions and two TA to relay the action potentials.

time through the path. An action potential from cell i will fail to propagate to cell j under the following circumstances:

- Cell j enters the upstroke phase during the conduction time.
- A recent propagation from cell j to cell i failed to stimulate cell i , i.e., a partial propagation, and the cells in between have not returned back to their resting phase.

To recognise these circumstances, the TA requires the following information of the cardiac cells (Figure 10):

- ap_i and ap_j : The phase of cell i and j 's action potential.
- $ap_i(t - \delta_{ij})$: The phase of cell i 's action potential when it reaches cell j after a conduction time of δ_{ij} .
- $ap_j(t - \delta_{ji})$: The phase of cell j 's action potential when it reaches cell i after a conduction time of δ_{ji} .

In addition, the local variable $last$ is needed to remember the direction of the last propagation:

$$last = \begin{cases} 0 & \text{if the last propagation was annihilated} \\ i & \text{if the last propagation started from cell } i \\ j & \text{if the last propagation started from cell } j \end{cases}$$

In Figure 15a, the left half of the TA determines if an action potential from cell i can propagate to cell j . The TA begins in the *idle* location and transitions to the *annihilate* location if both cells i and j go into the upstroke phase q_2 . A transition back to the *idle* location is made when both cells exit their upstroke phase q_2 . If only cell i goes into the upstroke phase q_2 , then a transition from the *idle* to *direction_i* location is made. Next, if a partial propagation from cell j occurred recently, then a transition to the *annihilate* location is made. Otherwise, a transition to the *wait_i* location is made. The TA transitions to the *annihilate* location if cell j enters the upstroke phase q_2 during cell i 's conduction time δ_{ij} . Otherwise, the TA remains in the *wait_i* location until the conduction time has elapsed, at which point the signal $start_i$ is emitted (denoted by “!”) and a transition to the *relay_i* location

is made. Next, a transition to the *idle* location is made after a time of δ_j has elapsed to ignore cell j 's upstroke phase. The right half of the TA uses similar logic to determine if an action potential from cell j can propagate to cell i .

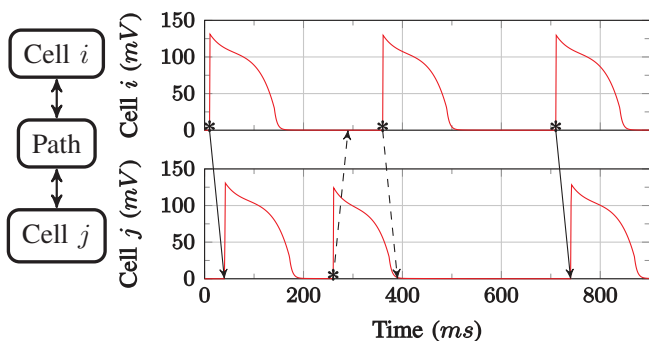
The TA in Figure 15b relays cell i 's action potential at cell j when the signal $start_i$ is received (denoted by “?”). The relay stops when cell j has successfully depolarised or when cell i 's action potential reaches the resting phase q_0 . Similar logic is used by the TA in Figure 15c to relay cell j 's action potential at cell i when the signal $start_j$ is emitted. A cell can be connected to multiple neighbours and, therefore, receive multiple action potentials simultaneously. We determine the voltage induced at cell k by its n neighbours with the following reaction-diffusion [10] function:

$$h_k(\vec{v}) = \sum_{i=1}^n \frac{\Gamma_{ik} \sigma_{ik}}{A_m C_m} (v_i^{out} - v_k) \quad (3)$$

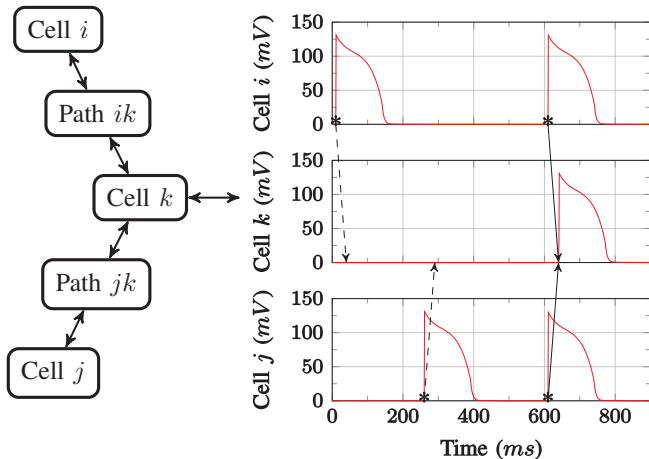
where Γ_{ik} is the cross-sectional area (units of mm^2) from cell i to k , σ_{ik} is the electrical conductivity (units of mS/mm) from cell i to k , A_m is cell k 's surface area to volume (units of mm^{-2}), C_m is cell k 's specific membrane capacitance (units of $\mu F/mm^2$), and v_i^{out} is cell i 's membrane potential after propagating along the path.

B. Discussion

We have developed an improved path model specifically for continuous-time action potentials. We can successfully model propagations that are annihilated by a full or partial propagation from the opposite direction. This allows us to model conduction block that only occur in one direction, e.g., due to the source-sink relationship [11], which the UPenn path model [7] can not. Bartocci et al. [31] modelled cardiac tissue with a high-resolution grid of Stony Brook cells [13]. In



(a) Full and partial propagations.



(b) Multiple neighbours needed to stimulate a cell.

Fig. 16. Examples of propagation behaviour that can be modelled by the improved path model, but not by the Oxford [6] or UPenn [7] path models.

that model, the cells are connected electrically by a reaction-diffusion equation because the conduction times between the cells are not significant.

Figure 16a demonstrates two cells i and j with a conduction block from cell j to i . The conduction time between the cells is 30ms . At 10ms , cell i generates an action potential that successfully stimulates cell j . At 260ms , cell j generates an action potential that does not stimulate cell i because of conduction block. Shortly after at 360ms , cell i generates an action potential that does not reach cell j because the cells along the path have not returned back to the resting phase q_0 . At 710ms , cell i generates an action potential that successfully stimulates cell j .

Figure 16b demonstrates a cell k that will only stimulate if the action potentials of its neighbours, cells i and j , arrive together. At times 10ms and 260ms , cells i and j , respectively, generate action potentials that take 30ms to propagate to cell k . However, the voltage induced on cell k is neither strong enough nor long enough to stimulate cell k . At time 610ms , both neighbours generate action potentials that arrive simultaneously at cell k . This time, the voltage induced on cell k is enough to stimulate it.

Figure 17 demonstrates atrioventricular node re-entrant tachycardia (AVNRT [12]), caused by dual pathways around the atrioventricular (AV) node shown in Figure 17a. An electrical stimulus propagates faster down the left pathway than the

right pathway, called the *fast* and *slow* pathways, respectively. In normal cardiac behaviour, shown in Figure 17a, an electrical stimulus from the atriums splits and propagates down the fast and slow pathways. The stimulus in the fast pathway will reach the bottom of the AV node before the stimulus in the slow pathway. The stimulus in the fast pathway continues to propagate down into the ventricles and up the slow pathway where it will annihilate the existing stimulus. Thus, only the stimulus that propagates down the fast pathway will enter the ventricles. Figure 17c demonstrates our ability to replicate this normal behaviour by modelling the dual pathways around the AV node with only four cells and paths.

An early electrical stimulus from the atriums can end up propagating continuously around the AV node, shown in Figure 17b. This is because the early stimulus cannot propagate down the fast pathway, which has cells that are still repolarising. The cells in the fast pathway take longer to repolarise than those in the slow pathway and, hence, have longer action potential durations. Due to this, the stimulus can propagate down the slow pathway because its cells have repolarised. By the time the stimulus reaches the bottom of the AV node, the cells in the fast pathway have reached their resting phase. Thus, the stimulus continues by propagating up the fast pathway, during which time the cells in the slow pathway reach their resting phase. The stimulus continues by propagating back down the slow pathway and the cycle continues. Every time the stimulus passes the bottom and top of the AV node, a stimulus is propagated into the ventricles and atriums, respectively. Figure 17d demonstrates our ability to replicate this abnormal behaviour by modelling the dual pathways around the AV node with only four cells and paths.

VI. UOA HEART MODEL

Following the approach of Oxford's heart model [6], we model the cardiac conduction system with a two-dimensional network of 33 cardiac cells, shown in Figure 1. Our heart model uses the improved cardiac cell and path models (Sections IV-B, IV-C, and V-A). The following cell and path model parameters were modified to capture the range of action potential durations, conduction velocities, and electrical conductivities present in the conduction system:

- The value of α_y^3 in Figure 10 was increased to increase the cell's rate of repolarisation and, therefore, decrease its action potential duration.
- The values of δ_{ij} and δ_{ji} in Figure 15 were increased to increase the conduction time and, therefore, decrease the conduction velocity.
- The value of σ_{ik} in equation (3) was increased to increase the conductivity.

Cardiac electrophysiology data in the literature [22], [32] was used to estimate the parameters. The data of interest include the morphology of myocyte action potentials and the conduction velocities of electrical stimuli along the pathways. Table IV provides a qualitative comparison of Oxford's heart model [6] with our improved heart model (UoA). Thanks to improvements in our cell and path models, we are able to model more heart conditions and with realistic results. This is

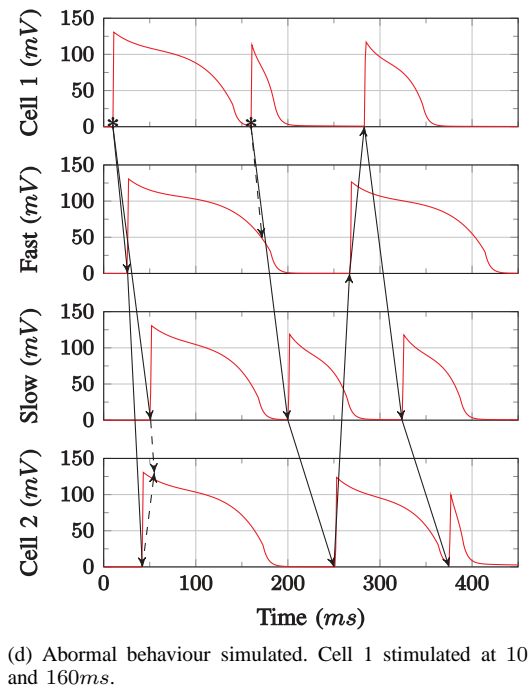
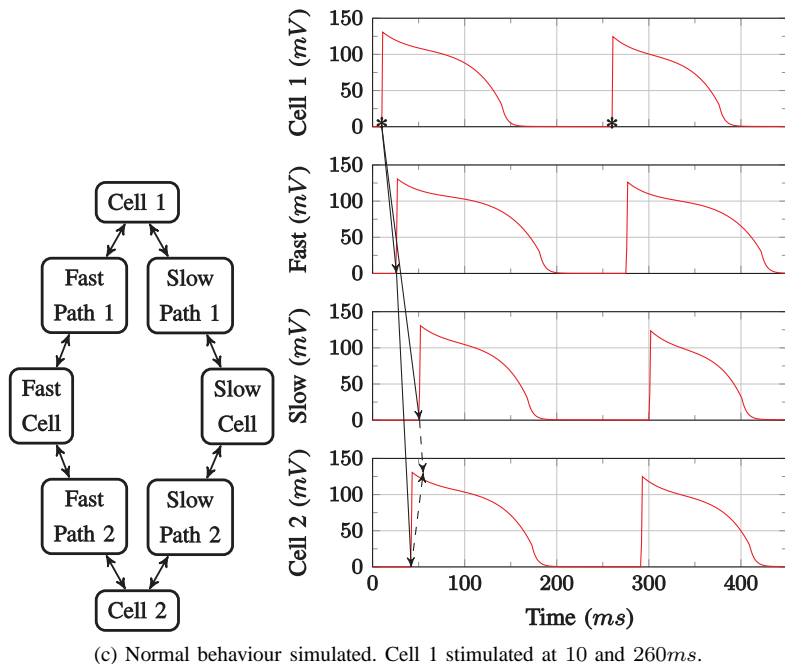
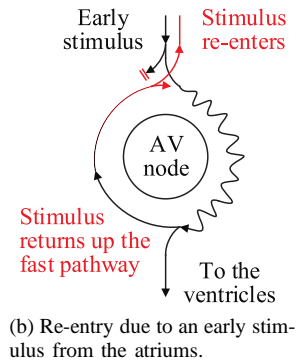
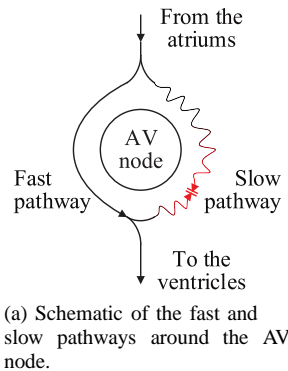


Fig. 17. Atrioventricular node re-entrant tachycardia.

demonstrated in the next section where we provide simulation results of the common arrhythmias described in Section II-D.

VII. SIMULATION RESULTS

We implemented our heart model in MathWorks[®] Simulink[®] and Stateflow[®] R2015b Pro. A fixed simulation time step of 0.0005ms and the Dormand-Prince ODE45 solver was used. Figure 19 shows the propagation of electrical stimuli through the cardiac conduction system (Figure 1) during a normal cardiac cycle. The membrane potential of each node is denoted by a shade of grey, according to Figure 18. In the following, we provide simulation results of the arrhythmias described in Section II-D.

A. Heart Block

This is modelled by reducing the voltage that the neighbouring atrial cells induce on the AV node and by increasing the conduction time through the AV node. Figure 20 shows a simulation of heart block where an electrical stimulus does not propagate through the AV node.

B. Bundle Branch Block

This is modelled similarly to heart block. For one of the bundle branches, the voltage induced by the AV node is reduced and the conduction time along the branch is increased. Figure 21 shows a simulation of bundle branch block where propagation down the right branch is slower than the left branch.

C. Long Q-T Syndrome

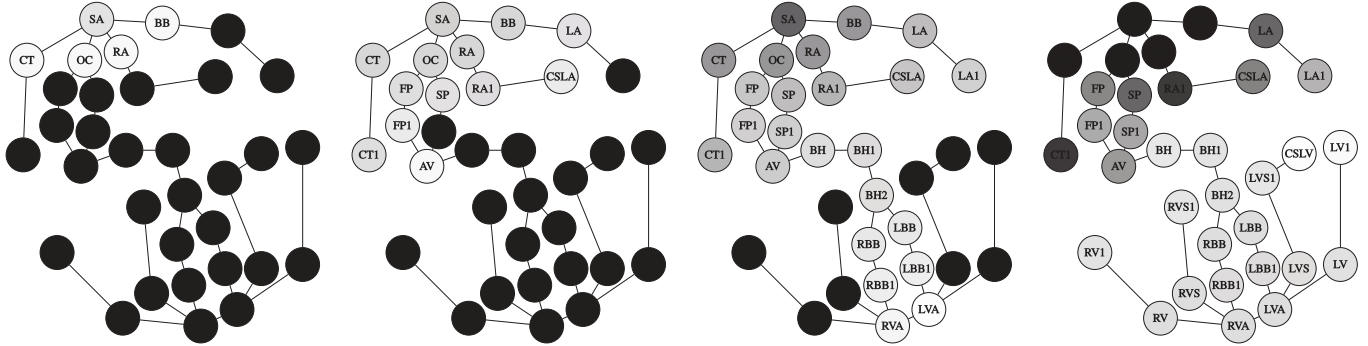
This is modelled by decreasing the value of α_y^3 in the ventricular cells to decrease their rate of repolarisation, thereby creating a longer action potential duration. Figure 22 shows a simulation of the syndrome.

D. VA Conduction

This is modelled by stimulating a ventricular node before the SA node generates a stimulus. Figure 23 shows a simulation of VA conduction by stimulating the RV1 node in the right ventricle.

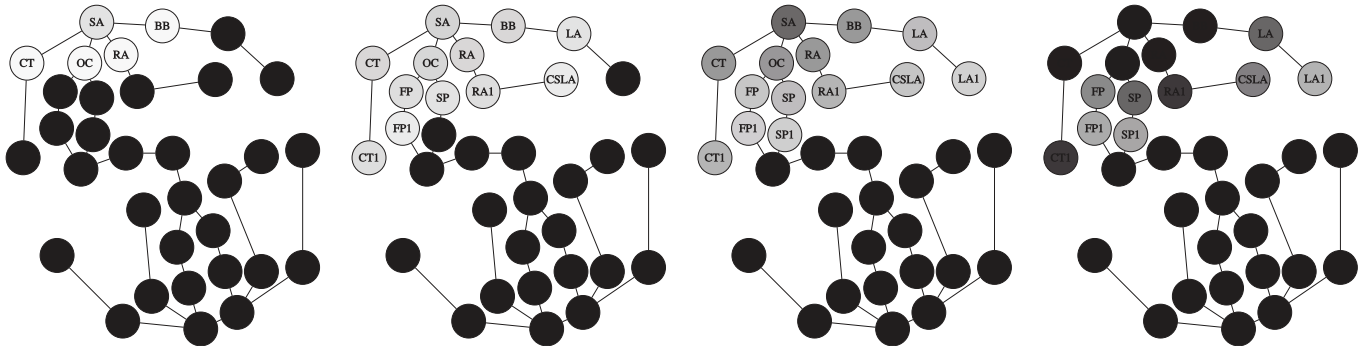


Fig. 18. Grayscale colourmap used to represent the voltage of each node.



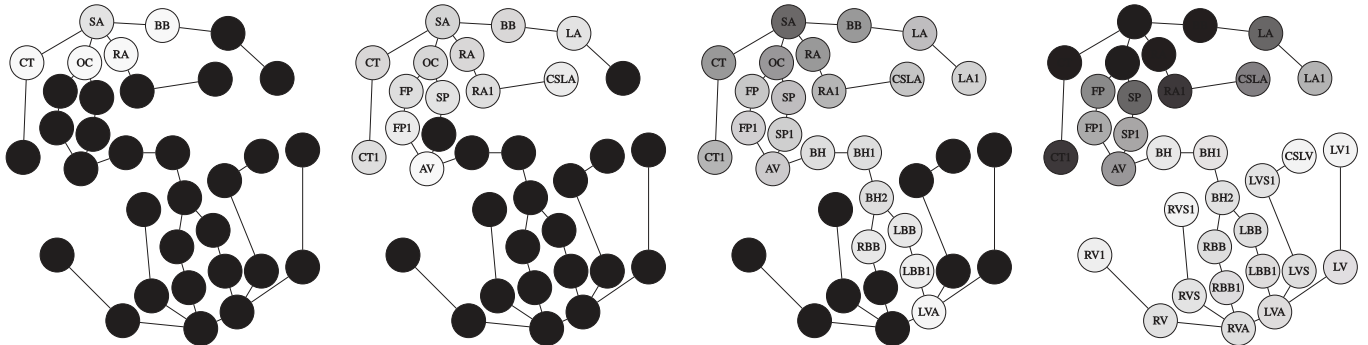
(a) 35ms. Electrical stimulus propagates from the SA node. (b) 88ms. Electrical stimulus arrives at the AV node. (c) 193ms. Electrical stimulus propagates into the ventricles. (d) 245ms. Electrical stimulus propagates up the ventricles.

Fig. 19. Simulation of a normal cardiac cycle. The SA node depolarises at 10ms.



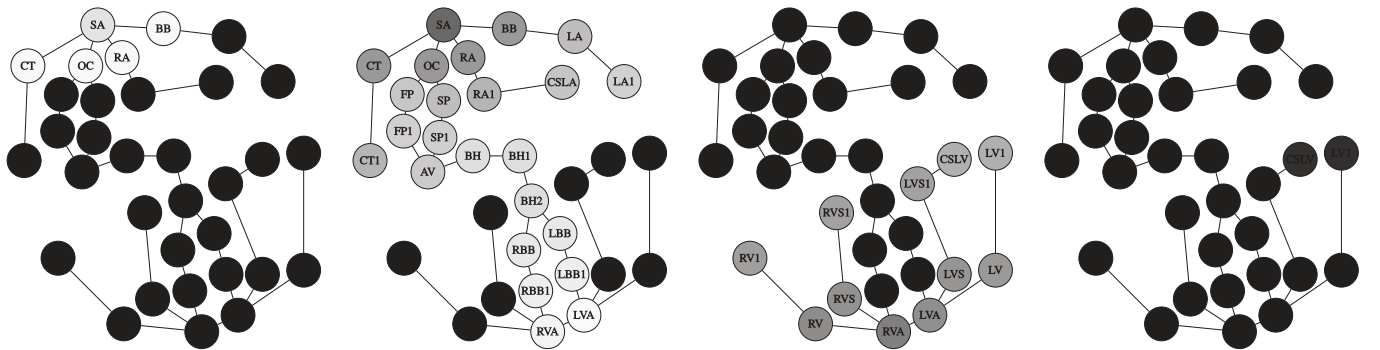
(a) 35ms. Electrical stimulus propagates from the SA node. (b) 88ms. Electrical stimulus is blocked at the AV node. (c) 193ms. Electrical stimulus fails to enter the ventricles. (d) 245ms. Ventricles fail to depolarise.

Fig. 20. Simulation of heart block. The SA node depolarises at 10ms.



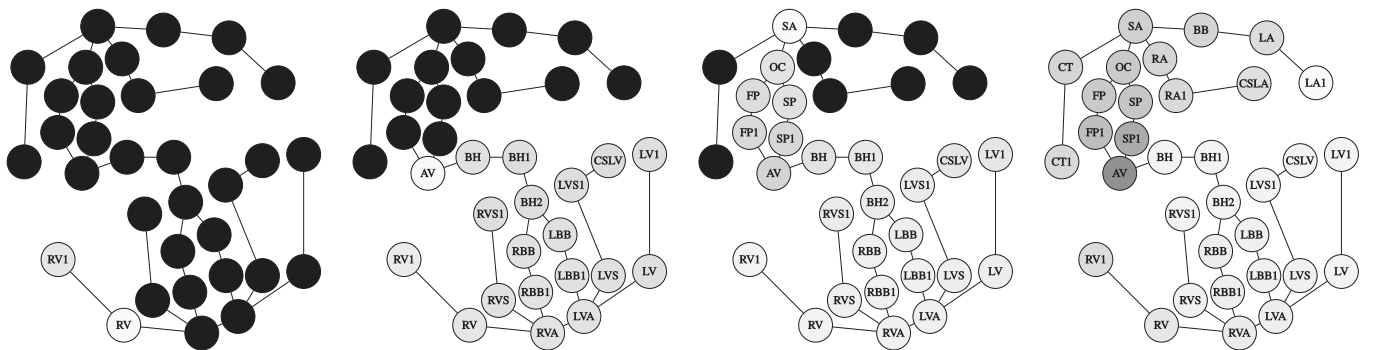
(a) 35ms. Electrical stimulus propagates from the SA node. (b) 88ms. Electrical stimulus arrives at the AV node. (c) 193ms. Electrical stimulus propagates slower into the right ventricle. (d) 245ms. Right ventricle depolarises after the left ventricle has depolarised.

Fig. 21. Simulation of right bundle branch block. The SA node depolarises at 10ms.



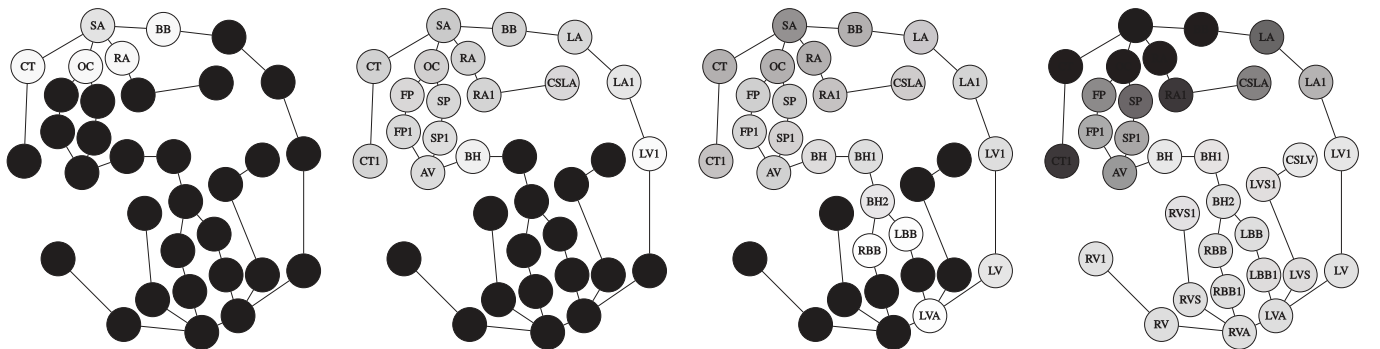
(a) 35ms. Electrical stimulus propagates from the SA node. (b) 193ms. Electrical stimulus propagates into the ventricles. (c) 640ms. Repolarisation of normal ventricles would already have completed. (d) 740ms. Repolarisation of the ventricles finally completes.

Fig. 22. Simulation of long Q-T syndrome. The SA node depolarises at 10ms.



(a) 35ms. Electrical stimulus propagates from the RV1 node. (b) 150ms. Electrical stimulus arrives at the AV node. (c) 220ms. Electrical stimulus propagates into the atrium. (d) 311ms. Electrical stimulus propagates down the atrium.

Fig. 23. Simulation of VA conduction. The RV1 node depolarises at 10ms.



(a) 35ms. Electrical stimulus propagates from the SA node. (b) 125ms. Electrical stimulus propagates into the left ventricle via the LA1 → LV1 accessory pathway. (c) 176ms. Left ventricle depolarises before the right ventricle. (d) 245ms. Ventricles have depolarised.

Fig. 24. Simulation of Wolff-Parkinson-White syndrome. The SA node depolarises at 10ms.

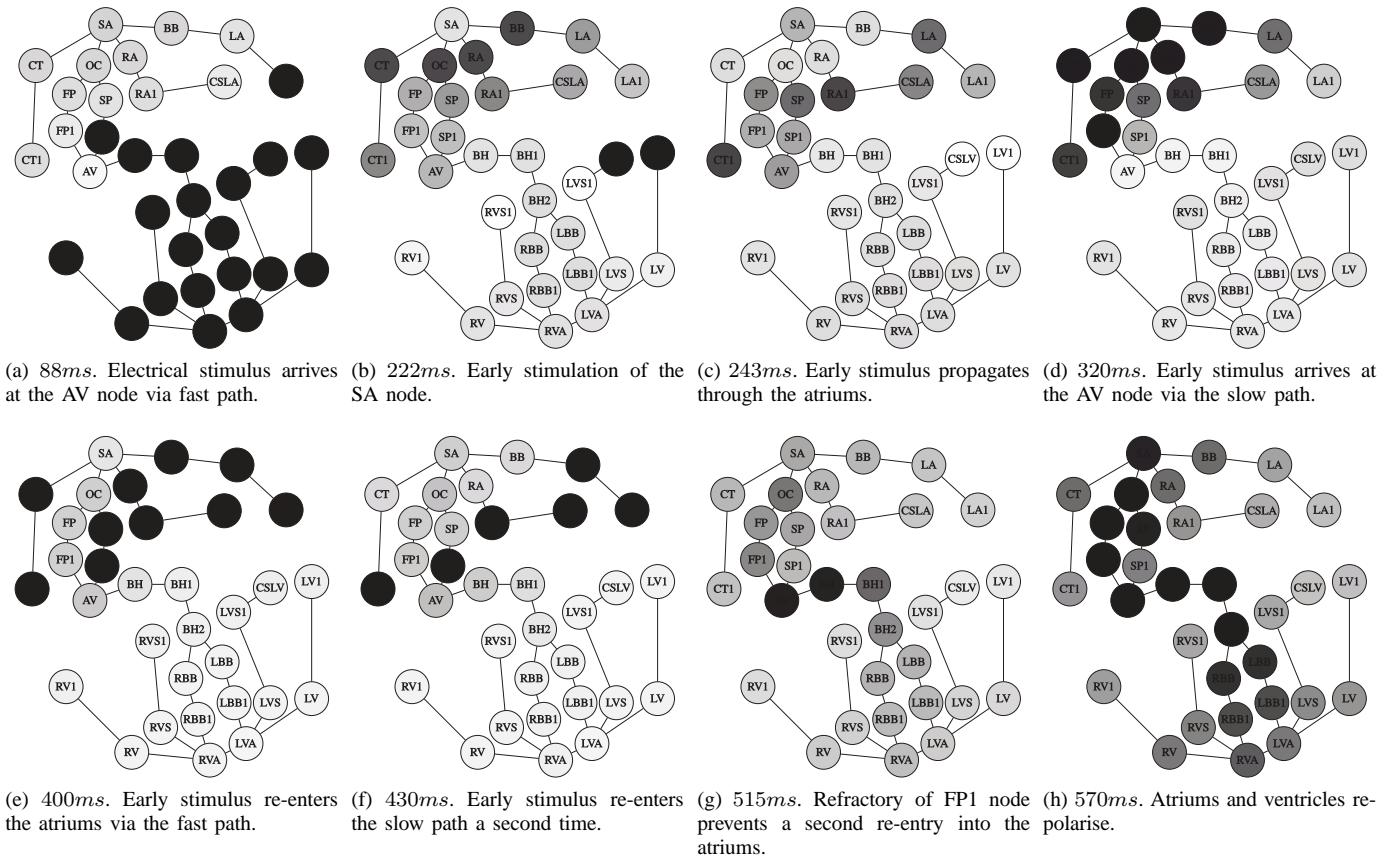


Fig. 25. Simulation of AV node re-entrant tachycardia. The SA node depolarises at 10 and 220ms.

TABLE IV
DETAILED QUALITATIVE COMPARISON OF HEART MODELS FROM UoA AND OXFORD.

	UoA	Oxford [6]
Heart Anatomy (Figure 1)	2D conduction system	
Morphology of action potentials (Figure 6)	Realistic because a more recent Stony Brook HA model [13] is used (with the improvements from Sections IV-B and IV-C)	Unrealistic because a simplified Stony Brook HA model [19] is used
Electrical Restitution (Figure 12)	Shows good dynamic behaviour	Shows limited dynamic behaviour
Path Model (Figure 16)	Electrical propagation is time delayed, bi-directional, and anisotropic.	
	Correctly disallows colliding electrical stimuli from passing through each other	Incorrectly allows colliding electrical stimuli to pass through each other
Disease Conditions (Figures 20 to 25)	Bradycardia and tachycardia by modifying the SA rate, AV node re-entrant tachycardia, VA conduction, heart blocks, and long Q-T syndrome	Bradycardia and tachycardia by modifying the SA rate, and heart blocks

E. Wolff-Parkinson-White Syndrome

This is modelled by creating an additional pathway between the left atrium and left ventricle. Figure 24 shows a simulation of the syndrome, which causes the left ventricle to depolarise earlier than usual.

F. AV Node Re-entrant Tachycardia

This is modelled by the fast and slow pathways around the SA node, demonstrated previously in Figure 17. Figure 25 simulates re-entrant tachycardia by stimulating the SA node a second time with an early stimulus.

G. Time to Simulate the Cell and Heart Models

The execution time needed to simulate the cell and heart models of Oxford and UoA are compared in this section. For a fair comparison, we wanted to avoid the execution overhead of the Simulink[®] environment. Thus, for each model, Simulink Coder[™] was used to generate a single-threaded executable C program that is optimised for execution speed. Each C program was then executed on a single core of a 3.40GHz Intel Core i7-4770 processor with 16GB of RAM and running Microsoft Windows 7 Enterprise. Each reported execution time is the average of ten runs of the same program.

The Oxford cell model takes 12.376s to simulate 60s of cell activity with a 1s base cycle length, compared with 9.586s for the UoA improved cell model. The Oxford cell

model takes longer to simulate because it uses a Stateflow[®] block to manually check the transition guards and produce a corresponding Boolean event whenever a guard is true. The Boolean event triggers another Stateflow[®] block to take transitions between the hybrid automaton states. For our UoA improved cell model, the hybrid automaton is modelled by a single Stateflow[®] block. The hybrid automaton transition guards are modelled directly as Stateflow[®] transition conditions. Stateflow[®] (automatically) handles the checking of transitions, which leads to a more efficient simulation, even though the Oxford cell model only uses the v_x variable of the Stony Brook 2005 cell model. Moreover, the UoA improved cell model uses Simulink[®] components that are more efficient to simulate wherever possible.

The Oxford and UoA heart models use the same arrangement of 33 nodes, as shown in Figure 1. The Oxford heart model has a total of 34 paths between the nodes and takes 8.516s to simulate 1s of a normal cardiac cycle. The UoA improved heart model has a total of 68 forward and backward paths between the nodes and takes 30.771s to simulate 1s of a normal cardiac cycle and 31.295s to simulate 1s of AV node re-entrant tachycardia. The UoA improved heart model takes longer to simulate because it implements a much more complex path model that considers the backward propagation and annihilation of electrical impulses throughout the cardiac conduction system. Thus, it is imperative to further improve the efficiency of the path model without sacrificing its predictive power. The execution time of the UoA improved heart model could be reduced by parallelising the simulation of the nodes over multi-cores [5].

VIII. CONCLUSION

We carefully reviewed the heart models designed for the closed-loop testing of pacemakers and identified key areas of improvement. To this end, we advanced the state-of-the-art in three ways: (1) stabilising and enforcing a minimum action potential duration on the Stony Brook cardiac cell model, (2) developing a path model that handles the partial and full propagation of continuous-time action potentials, and (3) demonstrating the predictive power of our heart model through the extensive simulation of arrhythmias. We are able to model many more arrhythmias than are possible with the existing heart models.

For future work, we look to implement our heart model with more computationally efficient methods to achieve the goal of real-time heart simulation, i.e., heart emulation. We also look to investigate the automatic generation and parameterisation of a network of cardiac cells and paths for patient-specific heart modelling.

ACKNOWLEDGMENT

This research was funded by the University of Auckland FRDF Postdoctoral grant No. 3707500. The authors would like to express their gratitude to Prof. Marta Kwiatkowsk and her research group from the University of Oxford for providing an implementation of their heart model.

REFERENCES

- [1] IEC 60601-1-11:2015, International Electrotechnical Commission Std. 2.0, Jan. 2015.
- [2] H. Alemzadeh, R. K. Iyer, Z. Kalbarczyk, and J. Raman, "Analysis of Safety-Critical Computer Failures in Medical Devices," *IEEE Security Privacy*, vol. 11, no. 4, pp. 14 – 26, 2013.
- [3] Z. Jiang, M. Pajic, and R. Mangharam, "Cyber-Physical Modeling of Implantable Cardiac Medical Devices," *Proceedings of the IEEE*, vol. 100, no. 1, pp. 122 – 137, Jan. 2012.
- [4] R. Bordas, B. Carpentieri, G. Fotia, F. Maggio, R. Nobes, J. Pitt-Francis, and J. Southern, "Simulation of Cardiac Electrophysiology on Next-Generation High-Performance Computers," *Philosophical Transactions of the Royal Society of London A: Mathematical, Physical and Engineering Sciences*, vol. 367, no. 1895, pp. 1951 – 1969, 2009.
- [5] E. Bartocci, E. M. Cherry, J. Glimm, R. Grosu, S. A. Smolka, and F. H. Fenton, "Toward Real-time Simulation of Cardiac Dynamics," in *Proceedings of the 9th International Conference on Computational Methods in Systems Biology*, ser. CMSB '11. ACM, 2011, pp. 103 – 112.
- [6] T. Chen, M. Diciolla, M. Kwiatkowska, and A. Mereacre, "Quantitative Verification of Implantable Cardiac Pacemakers over Hybrid Heart Models," *Information and Computation*, vol. 236, pp. 87 – 101, 2014, special Issue on Hybrid Systems and Biology.
- [7] Z. Jiang, M. Pajic, R. Alur, and R. Mangharam, "Closed-Loop Verification of Medical Devices with Model Abstraction and Refinement," *International Journal on Software Tools for Technology Transfer*, vol. 16, no. 2, pp. 191 – 213, 2014.
- [8] D. Méry and N. K. Singh, "Formalization of Heart Models Based on the Conduction of Electrical Impulses and Cellular Automata," in *Foundations of Health Informatics Engineering and Systems*, ser. Lecture Notes in Computer Science, Z. Liu and A. Wassyng, Eds. Springer Berlin Heidelberg, 2012, vol. 7151, pp. 140 – 159.
- [9] J. Lian, H. Krätschmer, and D. Müssig, "Open Source Modeling of Heart Rhythm and Cardiac Pacing," *The Open Pacing, Electrophysiology & Therapy Journal*, vol. 3, pp. 28 – 44, 2010.
- [10] A. G. Kléber and Y. Rudy, "Basic Mechanisms of Cardiac Impulse Propagation and Associated Arrhythmias," *Physiological Reviews*, vol. 84, no. 2, pp. 431 – 488, 2004.
- [11] P. Spector, "Principles of Cardiac Electric Propagation and Their Implications for Re-entrant Arrhythmias," *Circulation: Arrhythmia and Electrophysiology*, vol. 6, no. 3, pp. 655 – 661, Jun. 2013.
- [12] B. C. Mani and B. B. Pavri, "Dual Atrioventricular Nodal Pathways Physiology: A Review of Relevant Anatomy, Electrophysiology, and Electrocardiographic Manifestations," *Indian Pacing and Electrophysiology Journal*, pp. 12 – 25, Jan. 2014.
- [13] P. Ye, E. Entcheva, S. A. Smolka, and R. Grosu, "Modelling Excitable Cells Using Cycle-Linear Hybrid Automata," *IET Systems Biology*, vol. 2, no. 1, pp. 24 – 32, Jan. 2008.
- [14] C.-H. Luo and Y. Rudy, "A Dynamic Model of the Cardiac Ventricular Action Potential: I. Simulations of Ionic Currents and Concentration Changes," *Circulation Research*, vol. 74, no. 6, pp. 1071 – 1096, Feb. 1994.
- [15] T. J. Bunch, D. L. Hayes, C. D. Swerdlow, S. J. Asirvatham, and P. A. Friedman, *Pacing and Defibrillation: Clinically Relevant Basics for Practice*. Wiley-Blackwell, 2013, pp. 1 – 39.
- [16] C.-H. Luo and Y. Rudy, "A Model of the Ventricular Cardiac Action Potential: Depolarization, Repolarization, and Their Interaction," *Circulation Research*, vol. 68, no. 6, pp. 1501 – 1526, Jun. 1991.
- [17] F. Ou, "The Effects of Heart Structure on Action Potentials," Cardiac Electrophysiology Group, Auckland Bioengineering Institute, Tech. Rep., 15.
- [18] A. L. Hodgkin and A. F. Huxley, "A Quantitative Description of Membrane Current and its Application to Conduction and Excitation in Nerve," *The Journal of Physiology*, vol. 117, no. 4, pp. 500 – 544, 1952.
- [19] P. Ye, E. Entcheva, R. Grosu, and S. A. Smolka, "Efficient Modeling of Excitable Cells Using Hybrid Automata," in *Proceedings of Computational Methods in System Biology*, 2005, pp. 216 – 227.
- [20] F. Kusumoto, *Understanding Intracardiac EGMs and ECGs*, 1st ed. Wiley-Blackwell, 2010.
- [21] C. W. Haws and R. L. Lux, "Correlation Between In Vivo Transmembrane Action Potential Durations and Activation-Recovery Intervals From Electrograms. Effects of Interventions That Alter Repolarization Time," *Circulation*, vol. 81, no. 1, pp. 281 – 288, 1990.

- [22] D. Durrer, R. T. van Dam, G. E. Freud, M. J. Janse, F. L. Meijler, and R. C. Arzbaecher, "Total Excitation of the Isolated Human Heart," *Circulation*, vol. 41, pp. 899 – 912, Jun. 1970.
- [23] M. Sermesant, H. Delingette, and N. Ayache, "An Electromechanical Model of the Heart for Image Analysis and Simulation," *IEEE Transactions on Medical Imaging*, vol. 25, no. 5, pp. 612 – 625, May 2006.
- [24] B. H. Smaill and P. J. Hunter, "Computer Modeling of Electrical Activation: From Cellular Dynamics to the Whole Heart," in *Cardiac Electrophysiology Methods and Models*, D. C. Sigg, P. A. Iaizzo, Y.-F. Xiao, and B. He, Eds. Springer US, 2010, pp. 159 – 185.
- [25] R. Clayton, O. Bernus, E. Cherry, H. Dierckx, F. Fenton, L. Mirabella, A. Panfilov, F. Sachse, G. Seemann, and H. Zhang, "Models of Cardiac Tissue Electrophysiology: Progress, Challenges and Open Questions," *Progress in Biophysics and Molecular Biology*, vol. 104, no. 1 3, pp. 22 – 48, 2011.
- [26] A. A. McLeod and P. P. Jokhi, "Pacemaker Induced Ventricular Fibrillation in Coronary Care Units," *British Medical Journal*, May 2004.
- [27] P. C. Franzone, L. F. Pavarino, and S. Scacchi, Eds., *Mathematical Cardiac Electrophysiology*, ser. Modeling, Simulation & Applications. Springer International Publishing, 2014, vol. 13.
- [28] N. A. Trayanova, "Your Personal Virtual Heart," *IEEE Spectrum*, vol. 51, no. 11, pp. 34 – 59, Nov. 2014.
- [29] S. M. Green, A. J. Klein, S. Pancholy, S. V. Rao, D. Steinberg, R. Lipner, J. Marshall, and J. C. Messenger, "The Current State of Medical Simulation in Interventional Cardiology: A Clinical Document from the Society for Cardiovascular Angiography and Intervention's (SCAI) Simulation Committee," *Catheterization and Cardiovascular Interventions*, vol. 83, no. 1, pp. 37 – 46, 2014.
- [30] J. B. Nolasco and R. W. Dahlen, "A Graphic Method for the Study of Alternation in Cardiac Action Potentials," *Journal of Applied Physiology*, vol. 25, no. 2, 1968.
- [31] E. Bartocci, F. Corradini, M. R. D. Berardini, E. Entcheva, S. A. Smolka, and R. Grosu, "Modeling and Simulation of Cardiac Tissue using Hybrid I/O Automata," *Theoretical Computer Science*, vol. 410, no. 33 34, pp. 3149 – 3165, 2009.
- [32] D. C. Sigg, P. A. Iaizzo, Y.-F. Xiao, and B. He, Eds., *Cardiac Electrophysiology Methods and Models*. Springer US, 2010.



Eugene Yip received his B.E. (Hons) and Ph.D degrees in electrical and computer systems engineering from the University of Auckland, New Zealand. At the start of 2015, he joined the Heart-on-FPGA research group in the Department of Electrical and Computer Engineering, University of Auckland, as a research assistant working on the real-time modelling of cardiac electrical activity. In the middle of 2015, he joined the SWT research group at the University of Bamberg as a research assistant working on synchronous languages. His current research

interests include synchronous mixed-criticality systems, parallel programming, static timing analysis, formal methods for organ modelling, and biomedical devices.



Sidharta Andalam received his Ph.D degree from the University of Auckland, New Zealand, in 2013, where his thesis focused on developing a predictable platform for safety-critical systems. He is currently a research fellow in embedded systems at the University of Auckland, New Zealand. His principle research interest is in the design, implementation, and analysis of safety-critical applications. He has worked at TUM CREATE, Singapore, exploring safety-critical applications in the automotive domain.



Partha S. Roop received his Ph.D degree in computer science (software engineering) from the University of New South Wales, Sydney, Australia, in 2001. He is currently an Associate Professor and is the Director of the Computer Systems Engineering Program with the Department of Electrical and Computer Engineering, the University of Auckland, New Zealand. Partha is an associated team member of the SPADES team INRIA, Rhone-Alpes, France, and held a visiting position in CAU Kiel, Germany, and Iowa State University, USA. His research interests

include the design and verification of embedded systems. In particular, he is developing techniques for the design of embedded applications in automotive, robotics, and intelligent transportation systems that meet functional-safety standards.



Avinash Malik is a lecturer at the University of Auckland, New Zealand. His main research interest lies in programming languages for multicore and distributed systems and their formal semantics and compilation. He has worked at organisations such as INRIA in France, Trinity College Dublin, IBM research Ireland, and IBM Watson on the design and the compilation of programming languages. He holds B.E. and Ph.D degrees from the University of Auckland.



Mark Trew attained a Bachelor of Engineering in Engineering Science in 1992 and a Ph.D Engineering Science in 1999, both from the University of Auckland, New Zealand. He is currently a Senior Research Fellow at the Auckland Bioengineering Institute. Mark constructs computer models and analysis tools for interpreting and understanding detailed images of cardiac tissue and cardiac electrical activity.



Weiwei Ai received the B.S. degree in 2003 from Qingdao University, China, and the M.E. degree in 2006 from Beijing University of Technology, China. From 2006 to 2013, she worked as a reliability and failure analysis engineer in CEC Huada Electronic Design Co.,Ltd. She is currently working towards the Ph.D. degree at the the University of Auckland, New Zealand. Her research interests are in verification and validation with a focus on medical devices.



Nitish Patel received the B.E. degree from Mangalore University, Karnataka, India, and the Ph.D. degree from the University of Auckland, New Zealand. He is currently a Senior Lecturer at the University of Auckland. His research interests include embedded systems, robotics, artificial neural networks, control systems, and hardware implementation of real-time systems for control.